Article

Experimental and Analytical Characterization of Drop Impact Behavior for a Mobile Haptic Actuator

Byungjoo Choi [1], Jiwoon Kwon [2], Yongho Jeon [1] and Moon Gu Lee [1,*]

[1] Department of Mechanical Engineering, Ajou University, Suwon-si, Republic of Korea; dasom@ajou.ac.kr (B.C.); princaps@ajou.ac.kr (Y.J.)

[2] Department of Convergence Technology institute, Korea Construction Equipment Technology Institute, Gunsan-si, Republic of Korea; jwhj0814@gmail.com

[*] Correspondence: moongulee@ajou.ac.kr; Tel.: +82-31-219-2338

Abstract: Impact characterization of linear resonant actuator (LRA) is studied experimentally by newly developed drop tester, which can control various experimental uncertainty such as rotational moment, air resistance, secondary impact and so on. The feasibility of this test apparatus was verified by comparison with free fall test. By utilizing a high-speed camera and measuring the vibrational displacement of spring material, the impact behavior was captured and the damping ratio of the system was defined. Based on the above processes, the finite element model was established and the experimental and analytical results were successfully correlated. Finally, the damage of the system from impact loading can be expected by developed model and as a result, this research can improve the impact reliability of LRA.

Keywords: drop test; impact analysis; reliability; haptic actuator; linear resonant actuator (LRA)

1. Introduction

Haptic perception can be classified into kinesthesia and tactility. The kinesthesia senses the mass, hardness and shape of an object whereas tactility senses the roughness, protuberance and temperature of an object surface [1]. The haptic actuators which can communicate between a human and a machine based on the sense of touch are being developed ranging from smart devices to vehicles, game consoles, remote control and so on. Several studies are recently focused on how to make this technology more realistic and immersive. Therefore, its field of application is expected to expand further.

Many studies had carried out the technology related to haptic perception for decades ago. The use of an eccentric rotating motor (ERM) as a vibrational source was reduced because of lacking sensuous delivery caused by its slow response and narrow frequency range [2, 3]. The solenoid resonant actuator (SRA) and piezoelectric resonant actuator (PRA) were introduced as a fast and wide frequency response. However, the SRA was 25 mm or longer, making it too bulky to be applied to a small device, and the PRA required a high-voltage amplifier and lacked a structural durability because of the occurrence of piezoelectric effect at high voltages and their embrittlement. In recent year, consequently, the LRA with good durability and reasonable operating voltage has been used by employing a mechanical spring. It can achieve the fast response and wide vibrational frequency range by using a small-sized voice coil motor (VCM) [4].
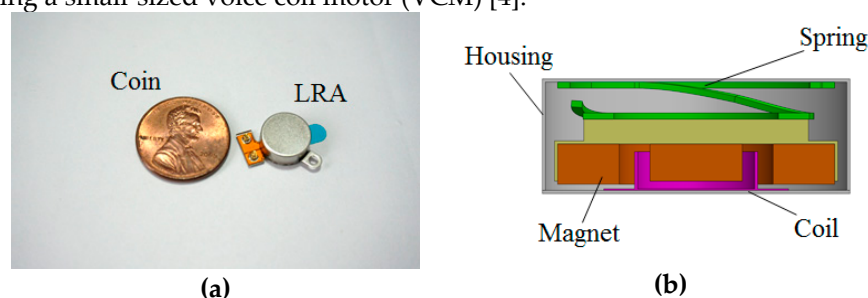
Figure 1. Appearance and internal structure of a coin-type LRA: (a) Appearance; (b) Cross-sectional view.

Figure 1 shows the structure of an LRA. A spring, magnet, and moving mass are fixed on the top of the housing, while the coil is attached at the bottom of the housing. When a current is applied to the coil, Lorentz force is generated due to the electromagnetic interaction between the current of the coil and magnetic field. This force results in haptic perception by vibration of the magnet and moving mass attached on the spring [5]. The structural durability of each component is a crucial part in the delivery of consistent haptic perception and therefore, related industry requires high reliability for this system. In the case of the impact durability test dropping from 1.8 m height, the only 10 % of malfunction rate for haptic actuator mounted in a smartphone is allowed in the industry. In order to satisfy this criterion, many suppliers have performed several research activities such as reliability test and analytical work. Despite those efforts, it is difficult to find a meaningful output for measuring the critical damage caused by impact force because a haptic actuator is extremely small size with a complicated internal structure. Among the components in the actuator, the spring is the most sensitive part under impact loading and the impact damage can change the natural frequency of the spring and this cause the malfunction like insufficient acceleration. Moreover, the identification and characterization of its mechanical behavior is very difficult because of its small size.

In this study, we developed the novel platform which can predict the mechanical damage for LRA under impact loading. To generate the impact loading, the specific drop tester was developed and the repeatability test was executed for checking the feasibility of the test apparatus. Also, the analytical model was established and appropriate material test was performed for obtaining the mechanical property simultaneously. As the relevance of the analytical model was proved by correlation with experimental result, we can successfully predict the mechanical damage of LRA under impact loading with developed analytical model finally. We can assure that the research output explained in this article can play a significant role for damage analysis of various electrical devices under impact loading.

2. Drop Tester

2.1. Drop tester configuration

In general, the falling motion of the mobile device shows several aspects by rotation moment, air resistance, secondary impact and so on. Therefore, it is very hard to analyze the mechanical behavior experimentally due to the experimental uncertainty caused by falling motion. In order to control the experimental uncertainty, the drop tester was newly developed

The experimental setup was constructed as shown in Figure 2. The impact force sensor (PCB, 200C50) is mounted onto the bottom part of the test system and the measured signal is acquired and saved by data acquisition system (LABVIEW). Also, the high-speed camera (FASCAM, APX-RS) was introduced for capturing the impact behavior visually and the image is captured in 512 × 512 resolution and 10,000 fps speed with LED light.
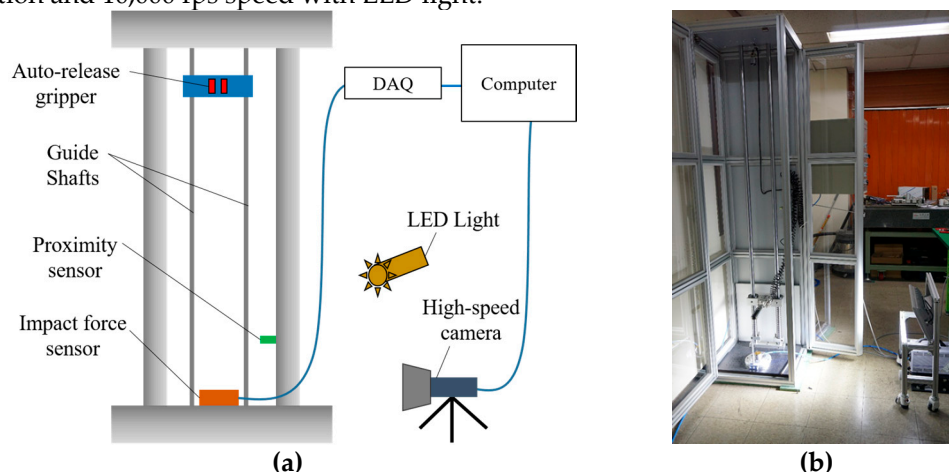
Figure 2. Drop tester configuration: (a) Schematic diagram; (b) Experimental setup.

The test specimen is fixed with an auto-release gripper, which is operated by pneumatic system, and the gripper is attached to the bushing. When the test begins, bushing starts the falling down through the guide shaft and then gripper releases the specimen passing the proximity sensor. Finally, the test object impacts the force sensor mounted onto bottom part of the impact tester. To reduce the experimental uncertainty especially friction during falling the object, bushing was composed of MC Nylon and grease was applied onto the guide shaft.

2.2. Drop tester verification

The developed drop tester consists of several supplementary components for controlling the experimental uncertainty and this supplementary component can distort the impact behavior. Therefore, the feasibility of this test apparatus must be verified by appropriated manner. In this study, we fulfilled the verification of this feasibility by comparison with free fall test. The slender rod was used as specimen and this rod was wrapped with silicone rubber to mitigate the vibration. Both rod with and without the constraint was dropped from 1.8 m height.
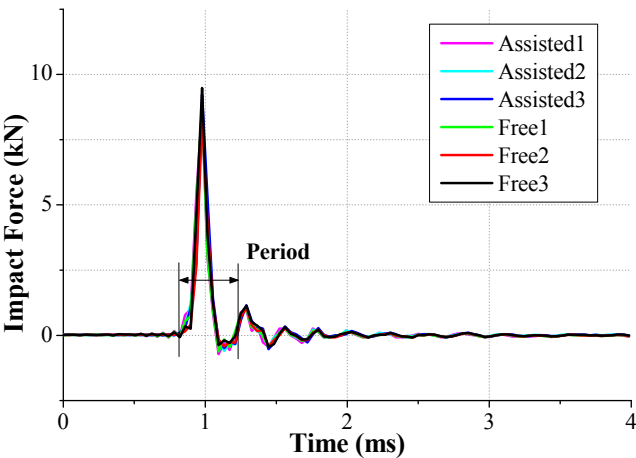

Figure 3. Comparison of generated impact force between the free and assisted test.

Table 1. The peak impact force and period from the free and assisted test.

	Peak Impact Force (kN)	Period (ms)	Force Error (%)
Assisted1	8.68	0.39	2.36
Assisted2	8.84	0.47	0.56
Assisted3	9.23	0.47	3.82
Free1	8.78	0.39	1.24
Free2	8.31	0.43	6.52
Free3	9.48	0.43	6.64

Despite the small allowable error in the peak force and period, as shown in Fig. 3 and Table 1, the primary impact and subsequent oscillation for both tests is well matched and the agreement between the free and assisted test suggests that the test result with newly developed test apparatus shows good repeatability.
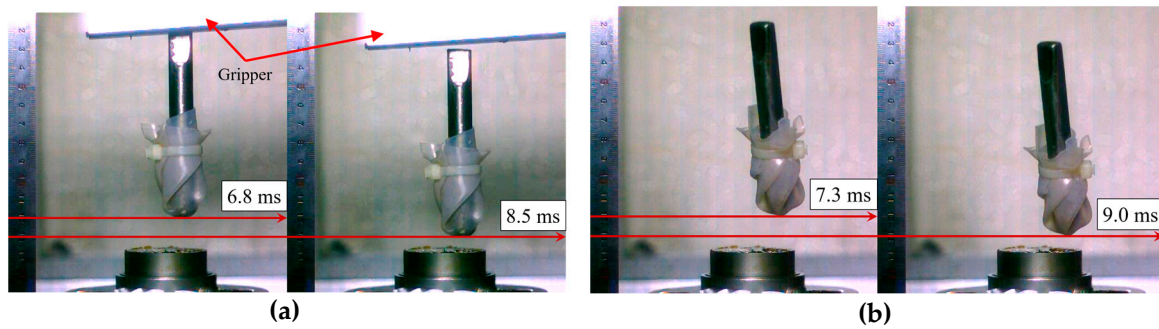
Figure 4. Comparison of falling velocity from the free and assisted test: (a) Assisted fall; (b) Free fall.

For comparison of the falling velocity just before the impact, the traveling time for 10 mm distance was measured with a high-speed camera and this is shown in Figure 4. The traveling time was estimated as 1.7 ms for both tests. Therefore, we can conclude that the falling velocity is 5.88 m/s and this velocity can be used as initial velocity for finite element analysis.

3. Finite Element Analysis of Impact Behavior of LRA

3.1. Determination of damping ratio for the spring

The damping ratio of mechanical components is a major factor for determining the magnitude of structural response under external loads. However, it is difficult to develop the constitutive model for structural damping because this is fully relied on the dynamic condition. In this study, we used the experimental approach rather than analytical approach to obtain the damping ratio of the spring. We applied a random excitation signal to spring and extracted the vibrational peak (x_i) and peak (x_{i+1}) at certain time. The logarithmic decrement method is helpful to obtain the damping ratio by applying the extracted peaks to following Eqs. (1) and (2) [6].
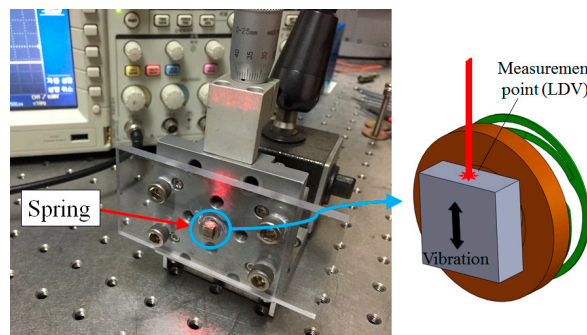
Figure 5. Experiment setup for measuring the vibrational behavior of the spring.
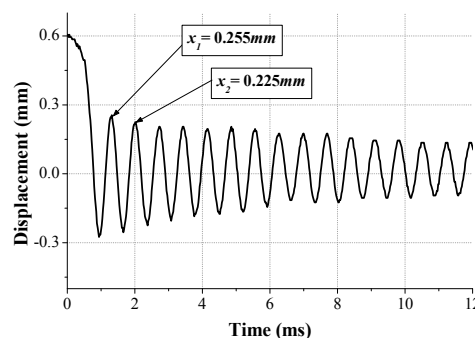

Figure 6. Measuring data for vibrational behavior.

$$\delta = \ln \frac{x_1}{x_2} \tag{1}$$

$$\xi = \frac{\delta}{\sqrt{(2\pi)^2 - \delta^2}} \tag{2}$$

Figure 5 shows experimental setup for measuring the vibrational behavior of the spring and the data is obtained by Laser Doppler Vibrometer (LDV). The direction of the vibration and excitation was matched with falling direction of the dummy phone. The measurement was run on a vibration isolation stage (Vibration isolation system, DAEIL SYSTEMS) to mitigate any vibrational noise and the data was acquired by an oscilloscope (Tektronix). As shown in Figure 6, the magnitude of first peak was 0.255 and second one is 0.225 and therefore the damping ratio (ξ) of the spring was eventually calculated as 0.02 using logarithmic decrement method.

3.2. Micro tensile test for spring
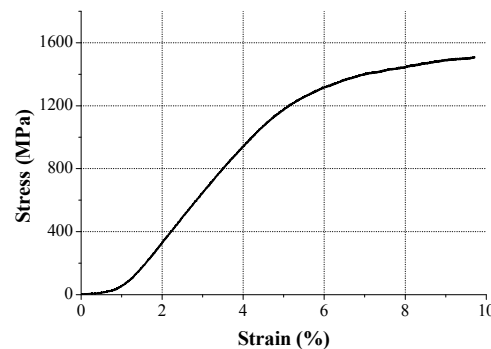
**Figure 7.** Stress–strain curve of SUS301 obtained by the micro tensile test.
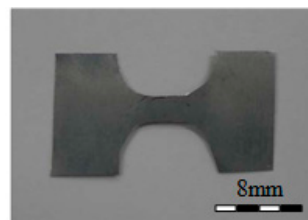
Figure 8. LRA spring test specimen.

The LRA spring used in this study is a thin plate which consists of 100 μm thick and 9 mm diameter and the mechanical property of the thin plate is quite different with bulk material as this can be changed by correlation of grain size with component size [7]. Therefore, the micro tensile test with specially prepared specimen was conducted to understand the mechanical property of the spring. The material of the specimen is SUS301 and this specimen was prepared with 200 μm thick, 3 mm gage length and 19 mm total length using photo etching. A universal material testing machine (UT-005, MTDI) was used in the micro tensile test and the stress-strain curve of the SUS301 is shown in Figure 7. Even though the ultimate tensile strength (UTS) of SUS301 is known as 1,300 MPa [8], the UTS in this micro tensile test is measured as 1510 MPa because of the size effect.

### 3.3. Experimental verification of analytical model

The drop test which is one of the experimental methods is the most accurate ways to study the impact resistance of a mobile devices. However, experimental approach cannot effectively characterize the impact behavior of each component because of its small size and behaving under high rate regime. In order to solve this issue, the finite element analysis was introduced in this study and this approach was verified by comparison with the experimental approach.
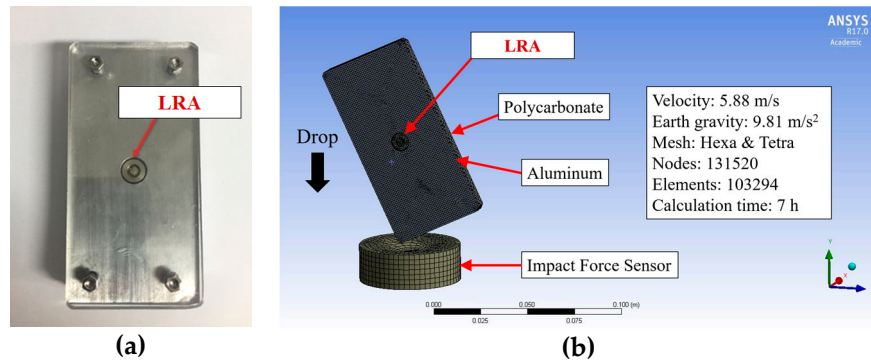
Figure 9. Physical and FE model of dummy phone with LRA: (a) dummy phone as test specimen; (b) finite element analysis.

To mimic the cellular phone, the appropriate dummy phone was prepared and the FE model was also generated for this physical model as shown in Figure 9. The dummy phone is composed of aluminum panel and LRA is attached to center of the panel. Also, this module is covered by transparent plate made of polycarbonate. This transparency allows the capturing the behavior of LRA by high-speed camera. The Hexa and Tetra element is applied as FE model element and the fine mesh with 60 μm element size is applied in the spring and moving mass which is our main interest. A falling velocity is applied as 5.88 m/s and gravitational acceleration is defined as 9.81 m/s². Also, the friction coefficient is applied as 0.61 for static and 0.47 for kinetic, respectively.
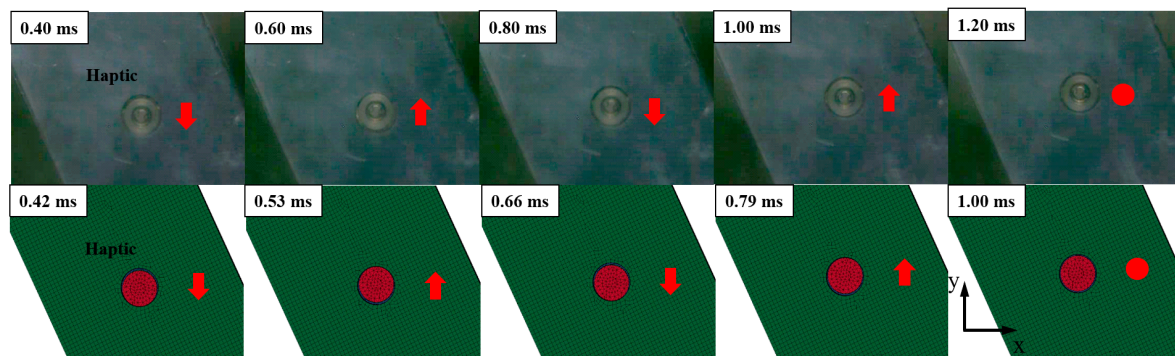
Figure 10. Impact behavior of LRA in the drop test and FE simulation.
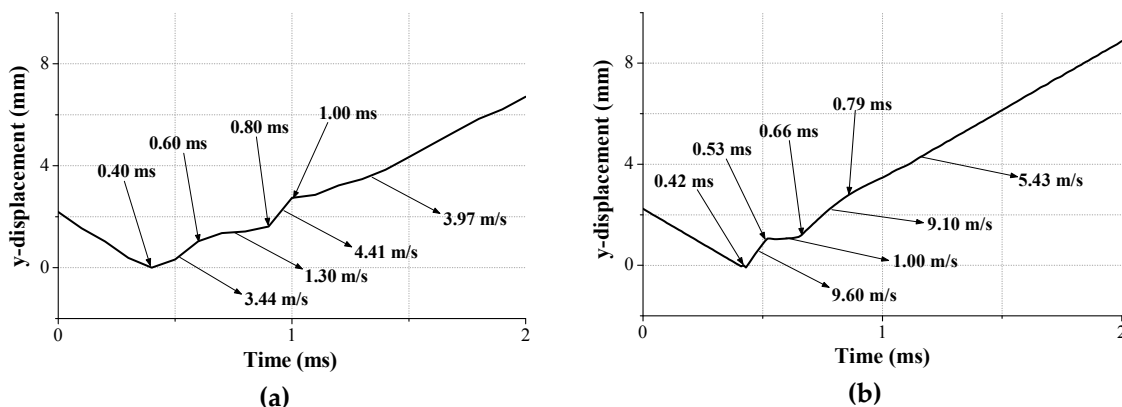
Figure 11. Comparison of traveling distance and moving velocity of the spring in the LRA: (a) Drop test; (b) FE simulation.

We can identify the rebounding behavior of moving mass from high-speed camera and FE simulation, as shown in Figure 10. The moving mass is oscillated with 0.40 ms period in the drop test whereas oscillating period is 0.24 ms in the FE simulation. Despite this discrepancy of the oscillating

period, we can insist that the FE model is valid for this application because the moving mass in both cases is stabilized after two period and rate dependency of the metallic structure can be negligible.

To clearly understand the validity of the FE simulation, the traveling distance of the moving mass is presented in Figure 11. We can confirm that the trend of both cases is well matched even though there is no energy dissipation in the FE simulation caused by perfectly elastic modeling.
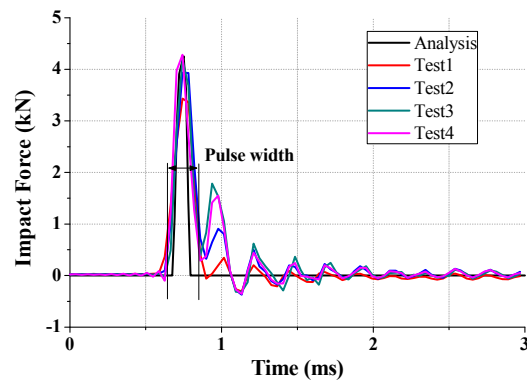

Figure 12. Impact force from drop test and FE simulation.

Table 2. Comparison of Impact force from the drop test and FE simulation.

	Peak Force (N)	Pulse Width (ms)
Analysis	4255.94	0.083
Test1	3433.23	0.128
Test2	3934.92	0.126
Test3	4186.65	0.118
Test4	4284.30	0.121

In spite of the short period of time, the estimation of accurate the impact force is very important because it can cause the external and internal damage for structure. Therefore, the agreement of the impact force from drop test and FE simulation must be checked. The peak force from drop test and FE simulation was measured and verify the validity of the analytical model as shown in Figure 12 and Table 2. The four tests were conducted and the average peak force was measured as 3959.78 N with 329.64 standard deviation. This value corresponds to the FE simulation results. On the other hand, it is consider that the small error (7.5%) is from drag and friction force.
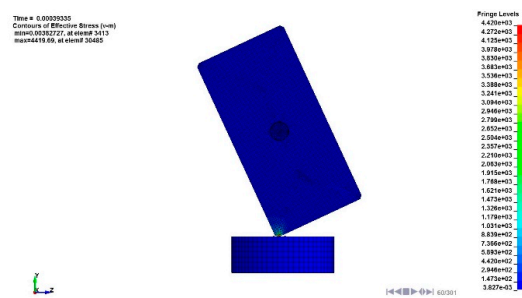
3.4. FE simulation

Figure 13. Stress (Von-Mises) contour from FE simulation under impact loading.

When the smart device such as smartphone drops on the floor, it starts the rotation due to rotational momentum generated by its asymmetric mass distribution. This rotation can raise up the uncertainty and make appropriate analysis difficult. Therefore, the rotational motion of the dummy

phone used in this study is restrained to avoid this uncertainty and to obtain the appropriate simulation result during FE simulation. In the FE modeling, the vertical line on the ground is considered as the datum line and the mass distribution of the dummy phone, which is impacted object, is bilaterally symmetrized with respect to this datum line. At the rebounding state, we can achieve the translational motion of impacted object without any rotational motion using this FE model. The stress contour from FE simulation is shown in Figure 13. The impact occurred at 0.33 ms and maximum stress was observed as 4420 MPa at 0.39 ms. The stress was concentrated at the vicinity of the impact point and this concentration phenomenon was verified as observing the damage in the experiment. At 0.46 ms, the impacted object began rebounding and the LRA including the moving mass and spring component started the oscillation. The traveling behavior of LRA spring attached to the impacted object is already shown in Figure 11 (b).
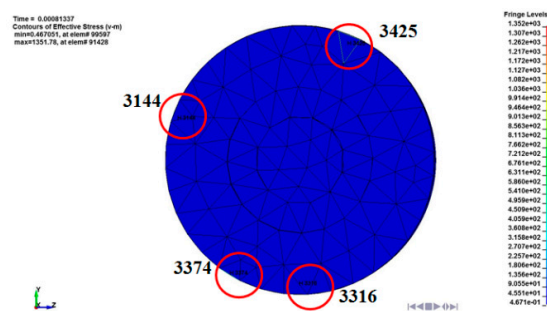

Figure 14. Contact element of moving mass fixed to the spring in the LRA.
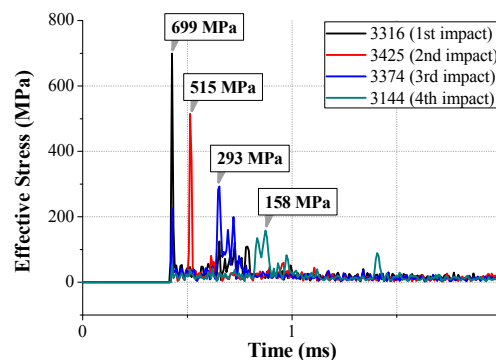
**Figure 15.** Impact stress (Von-Mises) generated in contact elements of the moving mass (from Figure 15)

In general, any component attached to traveling object subjected to perpendicular motion is expected to travel along the same direction with main object. In other words, the motion of the LRA can be expected as perpendicular motion to the ground in this case of study. In this FE simulation, however, the moving mass had asymmetrically oscillated to the datum line because of the asymmetricity of the spiral plaste spring fixed to the moving mass. Therefore, the impact between the moving mass and the LRA housing is also asymmetric. Even though the first impact occurred perpendicular to the ground between element 3316 and housing, all of the impact after the first one appeared the rotational motion to clockwise direction as shown in Figure 14. The impact stress of each element is shown in Figure 15 and the maximum stress is 699 MPa (0.43 ms), 515 MPa (0.51 ms), 293 MPa (0.65 ms), and 158 MPa (0.87 ms), respectively. This stress may cause the spring damage

.
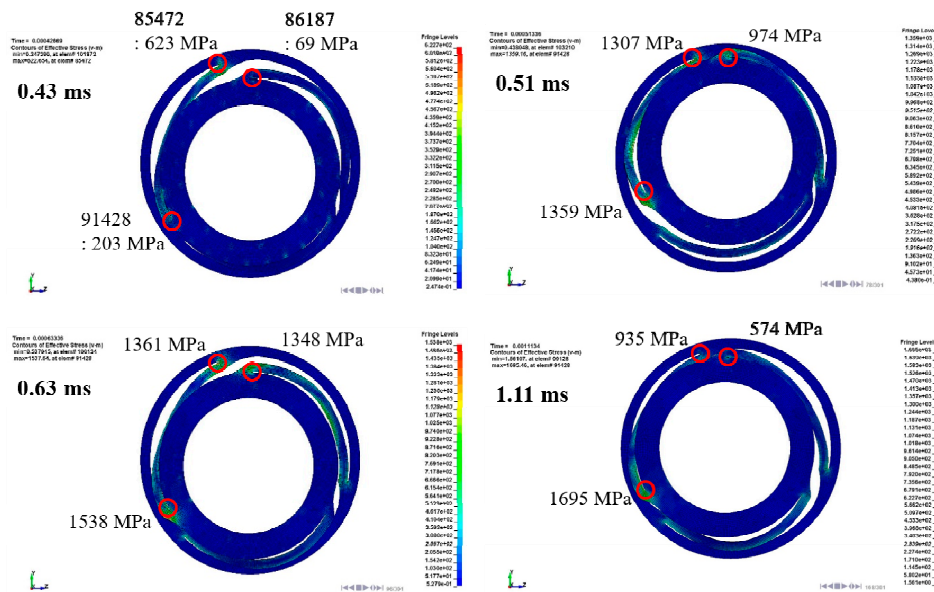
**Figure 16.** Impact stress (Von-Mises) and deformation of the spring in the LRA during impact loading.

In order to understand the spring behavior, the mechanical behavior of the spring was investigated. The stress and deformation state at a certain time is described in Figure 16. As mentioned above, the structural asymmetricity make the vibration skewing to the left. Because of the spring geometry, the stress was concentrated to the leg which is vicinity of supporting point and the maximum stress was observed at element 85472, 86187 and 91428 corresponding to each leg. The downward maximum deformation of spring was occurred at 0.43 ms. At that instant, element 85472 and 86187 were subjected to the tensile stress and the maximum stress was calculated as 623 MPa at the element 85472 whereas element 91428 was subjected to the compressional stress and the stress value is observed as 203 MPa. On the other hand, the upward maximum deformation of spring was occurred at 0.51 ms. At that instant, the stress state of each element was reversed and the stress value is magnified by stress accumulation. The stress value of element 85472 and 86187 was 1307 MPa and 974 MPa, respectively and the stress value of element 91428 was 1359 MPa. During the whole transient state, the maximum stress was occurred in the upward bouncing of the second period. The measured value was 1695 MPa which is over the UTS of the spring and therefore we can expect the severe damage of the spring [9].
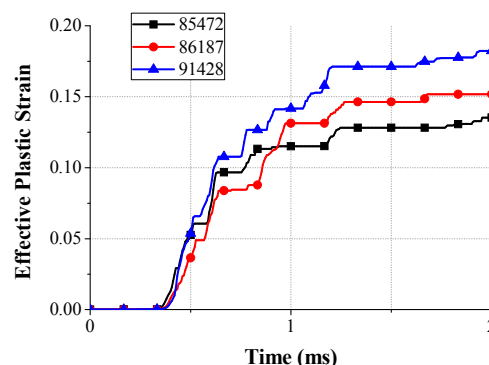
Figure 17. Effective plastic strain for certain elements in the spring during impact loading.

Figure 17 illustrates the effective plastic strain for certain elements subjected to concentrated stress. The plastic deformation began at 0.35 ms as the impact is transmitted to the spring. The initial strain slope of each element was similar but the strain is increased as order of high stress condition after first period (0.63 ms). Even the strain of element 86187 overtook the strain of element 85472 at 1.0 ms. This is because the accumulation and dissipation of the impact energy is different for each

element during transient state. The maximum strain was calculated as 0.135, 0.182, and 0.152 at element 85472, 91428, and 86187, respectively.
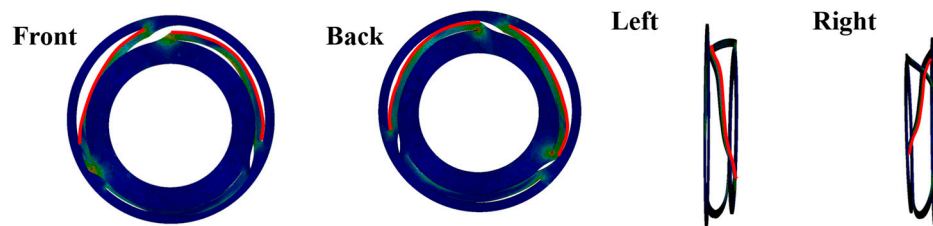
Figure 18. Expected deformation shape (highlighted with red lines) of the spring after the impact.

The expected deformation shape of the spring was calculated by FE simulation and this is illustrated in Figure 18. The upper plate, which is spring leg, is severely deformed and therefore, we can easily expect that the vibrational characteristic of the LRA is changed. This means that this LRA is no longer providing the haptic perception.

4. Conclusion

We developed the novel platform which can predict the mechanical damage for LRA under impact loading by using drop test and FE analysis methods.

(1) For the analysis, a series of preparation were carried out. First, the drop tester was newly developed for experimental verification of the FE model. Its experimental verification satisfied the free fall conditions while assisted drop with a test apparatus. Second, micro tensile test was performed to obtain the material properties considering the size effect of the thin LRA springs. Third, structural damping was modeled by measuring vibration displacement of a spring with random excitation signal.

(2) Based on the previous study, the impact FE modeling of dummy phone including LRA was performed. And its experimental verification was carried out by comparison of the impact deformation and force during the impact behavior. Despite the error in the impact force (7.5 %) and pulse width (33 %), the analytical model and experimental model were well correlated. Also, impact rebound displacement is well matched.

(3) Consequently, the damage of the FE model is analyzed. The external impact and secondary internal impact of LRA moving mass are concentrated on the LRA spring. Primary and secondary impact generated a maximum impact stress of 1695 MPa. Further, Effective strain at the same position was evaluated as 0.182. The damaged shape of the spring was confirmed and a vibration characteristic change were expected.

In conclusion, impact deformation and force were calculated through an experimentally verified FE model. This process can redeem the durability study against impact which has been conducted by designer's experience and trial-and-error. Finally, this research will be used extensively in impact analysis of smart devices, automobiles, medical devices, game machines, and remote controls, including small parts.

References

1.   Kern, T. A., "Engineering Haptic Devices," Berlin Heidelberg: Springer, 2009.
2.   Cho, Y. J., Yang, T. H., Kwon, D. S., "A New Miniature Smart Actuator based on Piezoelectric material and Solenoid for Mobile Devices," The 5th International Conference on the Advanced Mechatronics (ICAM), pp. 615-620, 2010.
3.   Yang, T. H., Pyo, D. B., Kim, S. Y., Cho, Y. J., Bae, Y. D., "A New Subminiature Impact Actuator for Mobile Devices," IEEE World Haptics Conference, pp. 95-100, 2011.

4.   Pyo, D. B., "A Novel Impact-Resonant Actuator for Mobile Devices," Master's Thesis, Korea Advanced Institute of Science and Technology (KAIST), Dae-Jeon, 2012.

5.   Kim, K. H., Choi, Y. M., Gweon, D. G., Lee, M. G., "A novel laser micro/nano-machining system for FPD process," Journal of Materials Processing Technology, Vol. 201, pp. 497-501, 2008.

6.   Inman, D. J., "Engineering Vibration," NJ: Pearson Education, 2008.

7.   Bazant Z. P., "Size effect on structural strength: a review," Archive of Applied Mechanics, Vol. 69, pp. 703-725, 1999.

8.   Gupta, R. K., Mathew C., Ramkumar P., "Strain Hardening in Aerospace Alloys," Frontiers in Aerospace Engineering, Vol. 4, No. 1, pp. 1-13, 2015.

9.   Magd, E. E., "Mechanical properties at high strain rates," Journal de Physique IV Colloque, Vol. 4, No. C8, pp. 149-170, 1994.

10. Goyal, S., Buratynski, E., "Methods for Realistic Drop-Testing," International Microelectronics and Packaging Society, Vol. 23, No. 1, pp. 45-52, 2000.

11. Kim, J. G., Lee, J. Y., Lee, S. Y., "Drop/Impact Simulation and Experimental Verification of Mobile Phone," Transactions of the Korean Society of Mechanical Engineers, Vol. 25, No. 4, pp. 695-702, 2001.

12. Kim, J. G., Park, Y. K., "Experimental Verification of Drop/Impact Simulation for a Cellular Phone," Experimental Mechanics, Vol. 44, No. 4, pp. 375-380, 2004.

13. Zhou, C. Y., Yu, T. X., Lee, S. W., "Drop/impact tests and analysis of typical portable electronics devices," International Journal of Mechanical Science, Vol. 50, pp. 905-917, 2008.

14. Karppine, J., Li, J., Pakarinen, J., Mattila, T. T., Paulasto-Krockel, M., "Shock impact reliablity characterization of a handheld product in accelerated tests and use environment," Microelectronics Reliability, Vol. 52, pp. 190-198, 2012.

15. Mattila, T. T., Vajavaara, L., Hokka, J., Hussa, E., Makela, M., Halkola, V., "Evaluation of the drop response of handheld electronic products," Microelectronics Reliability, Vol. 54, pp. 601-609, 2014.

16. Metz, R., "Impact and Drop Testing with ICP Force Sensors," Sound and Vibration, pp. 18-20, 2007.

17. Choi, B. J., Yeom, H. H., Jeon, Y. H., Lee, M. G., "Experimental verification of drop impact test and analysis for mobile electronics," The 11th International Conference on Multi-Material Micro Manufacture (4M) and the 10th International Workshop on Microfactories (IWMF), pp. 125-128, 2016.